Supplementary Information

Solution Catalytic Cycle of Incompatible Steps for Ambient Air Oxidation of Methane to Methanol

Benjamin S. Natinsky, Shengtao Lu, Emma D. Copeland, Jason C. Quintana, Chong Liu*

Department of Chemistry and Biochemistry, University of California, Los Angeles, California 90025, United States

*To whom correspondence may be addressed. Email: chongliu@chem.ucla.edu

Table of Contents

Chemicals and methods

Chemicals. The commercial reagents used in the various procedures were purchased from Sigma Aldrich, Alfa Aesar, Acros Organics, VWR and Fisher Chemicals unless otherwise noted; all chemicals were used as received unless specified. The deionized (DI) water that was used throughout the experiments came from a Millipore Milli-Q Water Purification System. The porphyrin ligands, protonated tetramesityl porphyrin (TMP)H_2 and protonated octaethyl porphyrin (OEP)H_2, were purchased from Frontier Scientific. 1,2-difluorobenzene (1,2-DFB) was purchased from Oakwood Chemical. The 1,2-DFB used in the glove box was distilled from CaH_2 and freeze-pump-thawed to remove residual O_2. The 1,2-DFB used in other experiments outside of the glove box was purified with activated 4 Å molecular sieves to remove residual moisture and methanol (CH_3OH) impurities. Tetrabutylammonium perchlorate ($TBAClO_4$), purified by recrystallization in ethanol (C_2H_5OH), was used as the electrolyte in all electrochemical measurements.

Chemical and materials characterizations. Spectra of one-dimensional proton nuclear magnetic resonance (^{1}H NMR) were recorded on a Bruker AV400 (400 MHz) spectrometer. The proton diffusion ordered spectroscopy (^{1}H DOSY) was performed on a Bruker AV300 (300 MHz) spectrometer. Chemical shifts for protons are reported in parts per million (ppm) and deuterated benzene (C_6D_6) and chloroform ($CDCl_3$) from Cambridge Isotope Laboratories were used as the locking solvents. ^{1}H NMR data are represented as follows: chemical shift, proton signal in molecule, multiplicity (s = singlet, d = doublet), coupling constants in Hertz (Hz), and integration. The mass spectral (MS) data were obtained on a Thermo Fisher Scientific Exactive series Direct Analysis in Real Time (DART) Mass Spectrometer. X-ray photoelectron spectroscopy (XPS) was measured on a Kratos Analytical AXIS Supra photoelectron spectrometer. The phosphorescence intensity measurements were conducted on a Leica SP8 SMD confocal laser scanning microscope. A JEOL JSM-6700F Field Emission scanning electron microscope (SEM) and a Zeiss Supra 40VP SEM were used to image the silicon (Si) nanowire arrays.

Synthetic procedures

(TMP)Rh−I (**1d**). This synthesis follows the procedure published by Wayland et al.[19] The solvent in this procedure, 1,2-dichloroethane (1,2-DCE), was freeze-pumped prior to use. In a four-neck flask equipped with an addition funnel and a reflux condenser, 250 mg of di-μ-chloro-tetracarbonyldirhodium(I) ($Rh_2(CO)_4Cl_2$), kept under inert atmosphere, was dissolved in 40 mL of

1,2-DCE and then added drop wise under dinitrogen (N_2) to a suspension containing 375 mg of (TMP)H_2 and 300 mg of anhydrous sodium acetate (CH_3COONa) dissolved in 200 mL of 1,2-DCE. The resulting solution mixture was refluxed at 90 ºC under N_2 for 48 hrs. After cooling to room temperature, I_2 was added in two stages: 100 mg initially and then 80 mg after 2 hrs. The reaction mixture was stirred at room temperature for 3 hrs after the second addition of I_2. The crude product was filtered to remove any insoluble inorganic salts, concentrated by rotary evaporation, and chromatographed on alumina by using $CHCl_3$ as the eluent. ^{1}H NMR (C_6D_6) (Figure S1): 8.77 (pyrrole H, s, 8H), 2.31 (*o*-CH_3, s, 12 H), 1.69 (*o*'-CH_3, s, 12 H), 7.18 (*m*-H, s, 4 H), 6.98 (*m*'-H, s, 4 H), 2.39 (*p*-CH_3, s, 12 H). DART MS: m/z = 1010.

(TMP)Rh−CH_3 (**1b**). This synthesis follows the procedure published by Wayland et al.[19] In a round bottom flask equipped with a reflux condenser, 50 mg of (TMP)Rh−I was dissolved in 25 mL of C_2H_5OH and warmed to 60 ºC for 40 min. The resulting solution was filtered and the filtrate was flushed with N_2 for 30 min. 7 mg of sodium borohydride ($NaBH_4$) dissolved in 2 mL of aqueous 0.5 M sodium hydroxide (NaOH) was added to the solution under N_2 and was stirred for 30 min. Addition of 0.1 mL of methyl iodide (CH_3I) resulted in the formation of an orange/red precipitate, which was collected via filtration. ^{1}H NMR (C_6D_6) (Figure S3): 8.69 (pyrrole H, s, 8 H), 2.20 (*o*-CH_3, s, 12 H), 1.68 (*o*'-CH_3, s, 12 H), 7.16 (*m*-H, s, 4 H), 7.03 (*m*'-H, s, 4 H), 2.39 (*p*-CH_3, s, 12 H), -5.31 (axial methyl, d, 3 H, 2.88 Hz). DART MS: m/z = 898.

(OEP)Rh−I (**2**). This synthesis follows the procedure published by Collman et, al.[32] Under N_2, 100 mg of (OEP)H_2 and 100 mg $Rh_2(CO)_4Cl_2$ were dissolved in 10 mL anhydrous dichloromethane (CH_2Cl_2). Then, 500 mg anhydrous CH_3COONa was added to the solution. Avoiding exposure to air, the stream of N_2 was adjusted such that the CH_2Cl_2 evaporated within 45 min. The resulting mixture was placed under vacuum for 10 min. This process of solvation with CH_2Cl_2, evaporation, and drying under vacuum was repeated. The resulting mixture was dissolved in 10 mL anhydrous C_6H_6 and, avoiding exposure to air, 100 mg I_2 was added. The reaction mixture was allowed to stir at room temperature for 20 min before the dry C_6H_6 was removed via rotary evaporation. The resulting mixture was chromatographed on silica by using CH_2Cl_2 as the eluent and then dried under vacuum. ^{1}H NMR ($CDCl_3$) (Figure S17): 10.28 (meso, s, 4 H), 4.19 (CH_2, m, 8 H, 6.5 Hz), 4.07 (CH_2, m, 8 H, 6.5 Hz), 1.96 (CH_3, t, 24 H, 6.5 Hz). DART MS: m/z = 763.

Si wire array. Si nanowire array applied in the bulk electrolysis was prepared following a modified electroless etching recipe based on the works by Huang et al.[29] A 4-inch, 500 μm thick, *p*-type boron-doped (100) Si wafer with an electrical resistivity of 0.01-0.02 Ω•cm (University Wafer, Inc.) was first sequentially rinsed with acetone, 2-propanol (IPA), and DI water, before being treated overnight in a piranha solution (3:1 H_2SO_4 (95-98%): H_2O_2 (30%)). The treated wafer was then etched in buffered HF (BHF) solution (10:1 NH_4F (40%):HF (49%)) to remove the native oxide, and exposed to O_2 plasma cleaning (Harrick Plasma, Plasma Cleaner PDC-32G) to remove organic residuals. The wafer was quickly transferred over to the etching solution ($AgNO_3$ and 5 M HF). To obtain nanowires of 15 μm length (Figure 4A), the wafer was etched for 3 hrs in 0.02 M $AgNO_3$ and 5 M HF. The duration of etching was minimized to 1 hr for nanowires of 10 μm in length (Figure S19A); 0.04 M $AgNO_3$ was utilized for a 3 hr etching process in order to prepare nanowires of 27 μm in length (Figure S19B) Afterward, 25% nitric acid (HNO_3) was added to dissolve the silver (Ag) deposited on the surface of the nanowires. Upon disposal of the HNO_3, the wafer was sequentially rinsed with DI water and acetone before drying. In the experiments of optical mapping of phosphoresce emission (Figure S8), Si wafer surface was patterned by photolithography with arrays of 4 μm-diameter dots of photoresist (AZ-5214-E) with 15 μm center-to-center distance between adjacent dots. Reactive ion etching was performed on the patterned wafer using a Versaline Fast DRIE system (Unaxis). After etching the remaining photoresist was removed using a Matrix-105 plasma asher (Matrix Integrated Systems). Before electrochemical testing, an ohmic contact between the Si electrode and a titanium foil was established with a combined use of Gallium-Indium eutectic, fast-drying Ag paint (Ted Pella, Inc.), and double-sided copper conductive tape (Ted Pella, Inc.). The passivation of residual negative charge on Si's surface was achieved by treating the electrode with the vapor of hexamethyldisilazane (HMDS) under slight vacuum, which allows the terminal surface Si−OH to react and yield Si−O−Si$(CH_3)_3$ moieties.[33] The electrode was used immediately for electrolysis after such a treatment.

Electrochemical characterizations

Cyclic voltammetry. Cyclic voltammograms were both performed inside a glove box under argon (Ar) and under atmospheric conditions with a Gamry Instruments Interface 1000-E potentiostat. All the solid chemicals used were dried under vacuum overnight prior to any testing. In a typical experimental condition, the electrolyte contains 0.1 M $TBAClO_4$ in 1,2-DFB, with a platinum (Pt)

wire as the counter electrode and a Ag^+/Ag pseudo-reference electrode equipped with a glass frit. A 2 mm diameter Pt working electrode was used in most cases. For electrochemical characterizations in air a 3 mm diameter glassy carbon working electrode was used to avoid the high reactivity of Pt with O_2 (Figure S2). Si wire array was also employed as the working electrode under Ar and in air in the presence of **1d** (Figure S9). The reported data are after *iR* correction. Cyclic voltammograms of decamethylferrocene were also conducted to calibrate the potentials of Ag^+/Ag pseudo-reference electrode, based on the reported standard potential of decamethylferrocene (−0.059 V vs. Saturated Calomel Electrode, SCE).[23]

Bulk electrolysis. The experiments of bulk electrolysis were performed using a Gamry Instruments Interface 1000-E potentiostat. A customized three-electrode electrochemical reactor with gas inlet/outlet ports was assembled as pictured in Figure S13. In a typical experiment, the electrochemical cell contains 0.1 M $TBAClO_4$ in 1,2-DFB, with a Pt wire as the counter electrode and a Ag^+/Ag pseudo-reference electrode with a glass frit. A mixture of CH_4 (Airgas, 99.5%) and house air were introduced into the reactor at a fixed ratio (P_{CH4}/P_{air}) under a constant flow rate with the use of mass flow controllers (Omega Engineering, Inc., Model: FMA5502A 0-10 sccm). The bulk electrolysis was conducted under a constant applied potential (E_{appl}) for varying durations. The procedures of *iR* correction and calibration of pseudo-reference electrode are similar as the ones in cyclic voltammetry. For the experiment of isotope labelling, bulk electrolysis was carried out with the same setup and procedure but with ^{13}C-labelled CH_4 (99 atom % ^{13}C, Sigma Aldrich). When needed, graphitic carbon cloth counter electrode was applied in place of the Pt wire counter (entry *3*, Table S1). Electrolysis with **1b** and flowing air was conducted in a three-electrode cell with glass carbon as the working electrode. When ethane (C_2H_6, 99%, Sigma Aldrich) and propane (C_3H_8, 98%, Sigma Aldrich) were introduced, the same setup and procedure as previous bulk electrolysis experiments were applied. Toluene ($PhCH_3$) was added in a concentration of 10 mM and a mixture of N_2 (Airgas, 99.999%) and air was fed into the reactor.

Stoichiometric reactions with 1b

Stoichiometric reactions between **1b** and different hydroperoxide species were performed and monitored by ^1H NMR. In one example, 0.25 mM **1b** and 0.25 mM *t*-butyl hydroperoxide were mixed in 1,2-difluorobenzene (1,2-DFB) for 6 hrs at room temperature. The ^1H NMR spectra in C_6D_6 indicate the formation of CH_3OH at the expense of the axial methyl group of **1b** (shown

below). Similar results were also obtained with cumene hydroperoxide in decane and 2-(1-hydroperoxy-1-methoxyethyl)-5-methylcyclohexan-1-ol in 1,2-DFB. The reaction between **1b** and *t*-butyl hydroperoxide is presented in Figure S4.

Product quantification

The products of CH_4 activation were quantified with a gas chromatograph equipped with a mass spectrometer (GC-MS, Agilent Technologies 5975 with Inert XL Selective Detector), owing to the interference of the $TBAClO_4$ electrolyte in the ^1H NMR spectra. A split/splitless injector was applied with a split ratio of 5:1 and a split flow of 5 mL/min. The instrument operated with an oven temperature of 50 ºC, an inlet temperature of 280 ºC, a column pressure of 16.08 psi, and a flow rate of 1.2 mL/min with helium carrier gas. A capillary HP-5MS column with 5% phenyl methyl siloxane (Model No.: 19091S-433, 30.0 m × 250 μm × 0.25 μm) was applied. The mass spectrometer had a source temperature of 230 ºC and a quadrupole temperature of 150 ºC. The injection volume was 1 μL and the injector was cleaned with $CHCl_3$ before and after each injection. For all analysis, samples were analyzed along with standards of known concentrations and the concentration of product in the analyzed samples is calculated based on the concurrent calibration curve (Figure S5).

CH_3OH was quantified at a retention time of ~2.71 min by the intensity of the 31 m/z peak, due to the interference of O_2 at m/z = 32. The detection limit of CH_3OH was found to be ~10 μM. In the case that $^{13}CH_4$ was introduced, the concentration of $^{13}CH_3OH$ was monitored with the peak of m/z = 33. Formaldehyde (HCHO) was monitored at a m/z ratio of 29 and quantified at a retention time of ~2.43 min with a detection limit of ~100 μM. Formic acid (HCOOH) was monitored at a m/z ratio of 46 and quantified at a retention time of ~2.51 min with a detection limit of ~100 μM. C_2H_5OH was monitored at a m/z ratio of 45 and quantified at a retention time of ~2.65 min with a detection limit of ~100 μM. 1-propanol was monitored at a m/z ratio of 31 and quantified at a retention time of ~2.90 min with a detection limit of ~100 μM. 2-propanol was monitored at a m/z ratio of 45 and quantified at a retention time of ~2.70 min with a detection limit of ~100 μM. Potential gaseous products including carbon monoxide (CO) and carbon dioxide (CO_2) were monitored on the same GC-MS instrument with a modified recipe. 2-mL gas samples were taken before and during the electrolysis and were manually injected into the GC-MS. Since the

instrument cannot differentiate the molecular ion peaks of CO and N_2, CO was monitored at the peak of m/z = 12. CO_2 was observed at its molecular ion peak of m/z = 44. Since CO_2 is present in the atmosphere, control samples were obtained to determine a baseline for the general CO_2 concentration. A calibration gas tank (Scott Mini-Mix) with 0.5 % CO, 0.5 % CO_2, 0.5 % O_2, and 0.5 % H_2 in N_2 was used to quantify the product. When $PhCH_3$ was used as the substrate, potential product benzyl alcohol was quantified by ^{1}H NMR. The peak at a chemical shift of ~4.4 ppm in C_6D_6 was integrated versus 1 mM internal standard tetramethylsilane. The concentration was determined based on an established calibration curve. Along the same lines, when *t*-butylbenzene was introduced as the substrate, ^{1}H NMR was also utilized to monitor the reaction at a chemical shift of ~1.8 ppm in C_6D_6 versus internal standard tetramethylsilane (TMS).

Numerical simulation

Experimental preparation for numerical simulation. The diffusion coefficients of compounds were determined in diffusion ordered spectroscopy (DOSY) on the Bruker AV300 spectrometer. One-dimensional ^{1}H NMR spectra were taken prior to determine and optimize spectral width, acquisition time, and the receiver gain. The DOSY spectra were obtained with a diffusion time (Δ) of 50 ms, a diffusion gradient length (δ) of 1.5 ms, a recycle delay between scans of 2 s, and the maximum gradient was 50 gauss·cm^{-1}. The spectra are reported in log of diffusion coefficient ($m^2 \cdot s^{-1}$) versus chemical shift (ppm). The diffusion coefficients were found to be 5.62×10^{-10} $m^2 \cdot s^{-1}$ for **1d** (Figure S6) and 1.75×10^{-9} $m^2 \cdot s^{-1}$ for ferrocene (Fc). The thickness of the diffusion layer in the setup of bulk electrolysis was determined by measuring the steady-state oxidation current of electrolyte with 1 mM Fc under the same condition of bulk electrolysis. The model of diffusion layer and the Fick's law of diffusion dictate[36]:

$$(I_{Fc} - I_{blank}) = AnFD\frac{C}{L_D} \quad (1)$$

Here I_{Fc} and I_{blank} are the steady-state oxidation currents at the same oxidation potential with and without Fc, respectively; A is the area of the electrode; F is the Faraday's constant; n = 1; D = 1.75×10^{-9} $m^2 \cdot s^{-1}$ for Fc; C = 1 mM; and L_D is the thickness of diffusion layer. The thickness of diffusion layer was calculated to be about 375 μm. This determined thickness of diffusion layer sets the boundary of computational model in numerical simulation below.

Numerical simulation. The finite-element simulations of a three-dimensional microkinetic model[37] were performed using COMSOL Multiphysics (Ver. 5.3). Two electrode geometries were simulated: a nanowire array and a planar electrode. The nanowire array had a fixed length of 50 μm and a diameter of 4 μm. A periodic boundary condition was applied parallel along the electrode surface, featuring a square array of wires vertical to the surface. The boundary of simulation perpendicular to the electrode is set to be the thickness of diffusion layer, L_D (375 μm). Convection and migration are not considered in the model. The periodicity of the array, p, defines the distance between the geometric center of adjacent wires. In the case of Figures S8 and 3B, p was set to 15 μm to reflect the wire array prepared in Figure S8, whereas in Figure S18B and S18C, p was varied to 20 and 30 μm to test the efficacy of the generated O_2 concentration gradient. The concentrations of species at the boundary of the diffusion layer and the initial concentration in the simulation are considered to be the bulk concentration of each species. The initial condition of the system contains 1 mM (TMP)Rh^{III+} and 0.97 mM O_2, which is calculated based on the solubility of O_2 in C_6H_6 with a partial pressure of 0.1 atm.[38] However, in Figure S18D and S18E, we studied the effect of the concentration gradients as the initial concentration of O_2 is increased to 2 and 4 mM, respectively. Based on our reaction model, we consider two electrochemical reactions taking place at the electrode surface:

Reaction 1 (*rxn 1*): electrochemical reduction of (TMP)Rh^{III+} to (TMP)Rh^{II} (**1a**)

Reaction 2 (*rxn 2*): electrochemical reduction of O_2 that is catalyzed by Rh porphyrin species

and one homogenous reaction taking place in the electrolyte:

Reaction 3 (*rxn 3*): solution bimolecular reaction between **1a** and O_2 that also eventually leads to the consumption of O_2

Based on the experimental data shown in Figure 2B, we assumed the equillibrium redox potentials for the reduction of Rh^{III} and O_2 occur at −1.26 V (*rxn 1*) and –1.0 V (*rxn 2*) vs. SCE, respectively. Concentration-dependent Butler-Volmer equations were applied to account for the electrochemical reactions on the materials' surface. Correspondingly, each reaction had a defined exchange current density ($i_{0,Rh}$ and $i_{0,O2}$ ($mA \cdot cm^{-2}$)) and *rxn 3* was taken to be an elementary reaction with second-order kinetics with a kinetic rate constant named as k_{O2} ($L \cdot mol^{-1} \cdot s^{-1}$). $i_{0,Rh}$ was limited to 1×10^{-6} $mA \cdot cm^{-2}$ to ensure that the simulation could converge. In addition, the second-order kinetic rate constant of reaction between **1a** and O_2 (k_{O2}) is set to be 10^6 $L^1 \cdot mol^{-1} \cdot s^{-1}$ in simulation results shown in Figures 3A and 3B, and Figure S18. Figure S7 describes the

modulation of the parameters $i_{0,O2}$ and k_{O2}, which cover 4 orders of magnitude, and the resulting concentration gradients that are induced. The diffusion coefficient for O_2 is set as 3.46×10^{-9} $m^2 \cdot s^{-1}$, the literature value of O_2 in C_6H_6.[39] The diffusion coefficient of $(TMP)Rh^{III+}$ as well as **1a** was set to be 5.62×10^{-10} m^2 $s^{-}1$, as determined experimentally using DOSY NMR.

***in situ* phosphorescence mapping**

An electrochemical setup with a microfluidic channel of about 200 μm thick (Figure S11) was constructed with a Pt wire was used as the counter electrode and a Ag wire as the pseudo-reference electrode. The setup was mounted on the slide holder of a reverted confocal laser scanning microscope (Leica SP8 SMD). A 526 nm line of the white light laser was used as the excitation source and the phosphorescent emission between 570 – 750 nm was collected for confocal imaging with a 20 × 20 immersion type objective lens. The confocal scan works on the x-z-t mode at a spatial resolution of 146 nm/pixel, over an area of 150 μm × 150 μm *x-z* cross-section with a time-lapse of 0.361 frame s^{-1}.

Calculations of equivalent turnover numbers (TON and TON') and kinetic rate constants

Equivalent TON. The equivalent TON is defined as the number of product molecules generated per total catalyst in the system. The amount of active catalyst, **1a**, is taken as the amount of pre-catalyst, **1d**, added into the system. This approximation may significantly over-estimate the amount of active catalyst therefore the equivalent TON may be underestimated.

Equivalent TON'. The equivalent TON' is defined as the number of product molecules generated per catalyst molecule within the nanowire array. As the CH_4-reactive **1a** is only existent within the nanowire array due to the concentration gradient, we assume only the solution within the nanowire array are catalytically active. Furthermore, we approximate the bulk concentration of **1d** as the steady-state concentration of **1a** during catalysis. This approximation may over-estimate the amount of active catalyst therefore the equivalent TON' may be underestimated.

Kinetic rate constants of C−H activation. As the step of C−H activation was shown to be turnover-limiting in the proposed catalytic cycle, the kinetic rate constant of C−H activation in the wire array ($k_{f,nano}$) can be calculated based on rate of product accumulation in the catalysis. Moreover, assumptions of the active catalyst similar to the case of calculating TONs are made, which implies that the reported values of $k_{f,nano}$ may be underestimated. Last, experiments of ^1H NMR was used

to determine the solubility of gaseous substrates under a certain partial pressure. The resultant concentrations of substrates at 1-atm partial pressure are: [CH_4] = 9.54 mM, [C_2H_6] = 119 mM, and [C_3H_8] = 235 mM. Additionally, [$PhCH_3$] = 10 mM as dictated by the experimental condition.

Safety Statement. No unexpected or unusually high safety hazards were encountered.

Table S1. Experimental results of bulk electrolysis in this work

Entry	Pre-catalyst	Duration (hrs)	Substrates	Gas composition [a]	Electrode	Product	[Product] (mM)	TON [b] Avg in solution	TON' [c] Avg in array
1	–	3	1 mM **1b**	N_2/air (35:1)	Glassy carbon	CH_3OH	1.30±0.36 [d]	–	–
2	1 mM **1d**	3	CH_4	CH_4/air (35:1)	15-µm Si NW	CH_3OH	0.37±0.20	0.37	2972
3 [e]	1 mM **1d**	3	CH_4	CH_4/air (35:1)	15-µm Si NW	CH_3OH	0.39	0.39	3133
4	1 mM **1d**	6	CH_4	CH_4/air (35:1)	15-µm Si NW	CH_3OH	0.92±0.06	0.92	7390
5	1 mM **1d**	9	CH_4	CH_4/air (35:1)	15-µm Si NW	CH_3OH	1.48±0.06	1.44	12771
6	1 mM **1d**	24	CH_4	CH_4/air (35:1)	15-µm Si NW	CH_3OH	6.45±0.92	6.45 [f]	51807 [f]
7	–	3	CH_4	CH_4/air (35:1)	15-µm Si NW	None	–	–	–
8	1 mM **1d**	3	CH_4	CH_4 in Ar [g]	15-µm Si NW	None	–	–	–
9	1 mM **1d**	3	–	N_2/air (35:1)	15-µm Si NW	None	–	–	–
10	1 mM **1d**	3	$^{13}CH_4$	$^{13}CH_4$/air (35:1)	15-µm Si NW	$^{13}CH_3OH$	0.46	0.46	3694
11	1 mM **1d**	3	C_2H_6	C_2H_6/air (29:1)	15-µm Si NW	C_2H_5OH	1.49	1.49	11968
12	1 mM **1d**	3	C_3H_8	C_3H_8/air (12:1)	15-µm Si NW	C_3H_7OH	0.32	0.32	2570
13	1 mM **1d**	3	10 mM $PhCH_3$	N_2/air (35:1)	15-µm Si NW	$PhCH_2OH$	1.22	1.22	9799
14	1 mM **1d**	3	10 mM *t*-butylbenzene	N_2/air (35:1)	15-µm Si NW	None	–	–	–
15	0.5 mM **1d**	6	CH_4	CH_4/air (35:1)	15-µm Si NW	CH_3OH	0.15±0.07	0.30	602
16	1 mM **2**	3	CH_4	CH_4/air (35:1)	15-µm Si NW	None	–	–	–
17	1 mM **1d**	3	CH_4	CH_4/air (35:1)	Si planar electrode	None	–	–	–
18	1 mM **1d**	3	CH_4	CH_4/air (35:1)	50-µm Si array [h]	None	–	–	–
19	1 mM **1d**	3	CH_4	CH_4/air (1:1)	15-µm Si NW	None	–	–	–
20	1 mM **1d**	3	CH_4	CH_4/air (>1000) [i]	15-µm Si NW	CH_3OH	0.25	0.25	2008
21	1 mM **1d**	3	CH_4	CH_4/air (35:1)	10-µm Si NW	CH_3OH	0.19	0.19	2289
22	1 mM **1d**	3	CH_4	CH_4/air (35:1)	27-µm Si NW	CH_3OH	0.45	0.45	1807
23	–	3	CH_4	CH_4/air (35:1)	"Spent" 15-µm Si NW [j]	None	–	–	–
24	1 mM **1d**	3	CH_4	CH_4/air (35:1)	Passivated 15 µm Si NW [k]	None	–	–	–

General conditions: 0.1 M $TBAClO_4$ in 1,2-DFB, E_{appl} = −1.4 V vs. SCE. The products are considered as "none" when the concentration of the potential products is below the instrument detection limit (~ 0.01 mM). NW, nanowire array. Error denotes SEM; n = 2 or 3 when errors were noted. [a] The value in the bracket is the ratio of partial pressure between the two gases, if applicable. When CH_4 and air were used, the ratio is denoted as P_{CH4}/P_{air} in the main text. [b] TON, turnover number, calculated as the concentration of CH_3OH divided by concentration of pre-catalyst **1d**. [c] TON' is calculated as the moles of generated CH_3OH divided by moles of pre-catalyst **1d** within the nanowire array. [d] Solvent evaporation during the bulk electrolysis leads to a slight over-estimation about the concentration of the yielded CH_3OH. [e] Plain carbon cloth was used as the counter electrode in place of a Pt wire. [f] Significant solvent evaporation was observed within 24 hrs. The values was calculated by taking this into account. [g] Conducted in an Ar glove box with the addition of 10 mM de-ionized water. [h] Si wire array, periodicity is 15-μm, length is 50-μm, and diameter is 4-μm which is shown in Figure S12. [i] Trace atmospheric O_2 was used. [j] The electrode is a spent Si nanowire electrode that was used in a previous 3-hr bulk electrolysis at the same condition in entry *2* which yielded CH_3OH. [k] Si nanowire electrode was pre-treated with HMDS vapor before bulk electrolysis. The HMDS treatment passivates the negative charge on the Si's surface.

Table S2. Reactivities of reported homogeneous catalysts for methane functionalization

Catalyst	Liquid media	Temperature (°C)	P_{CH4} (psi)	Oxidant or reactant	Product	Yield (%)	Selectivity (%)	TOF [a] (hr^{-1})	TON [b]	Ref.
K_2PtCl_4	20% SO_3/H_2SO_4	215	943	SO_3	CH_3OSO_3H	–	98	24100	–	(*40*)
$Tl(TFA)_3$ [c]	$HTFA_{(l)}$ [c]/$CH_{4(g)}$	180	500	$Tl(TFA)_3$ [c]	CH_3TFA [c]	74	100	–	–	(*41*)
$PdSO_4$	96% H_2SO_4	180	400	SO_3	CH_3OH [d]	10 [e]	17	~3.6	18 [e]	(*42*)
$PdSO_4$ [f]	H_2SO_4	140	500	Echem [f]	– [g]	–	–	2000	–	(*8*)
$PdSO_4$ [h]	20% SO_3/H_2SO_4	70	500	Echem [h] & SO_3	CH_3OSO_3H & CH_3SO_3H	46 [i]	NA	–	~ 10	(*8*)
$HgSO_4$	100% H_2SO_4	180	500	SO_3	CH_3OSO_3H	43	85	~3.6	NA	(*5*)
$Au_2(SO_4)_3$	96 % H_2SO_4	180	390	H_2SeO_4	CH_3OSO_3H	NA	77	~3.6	32	(*7*)
$(bpym)PtCl_2$ [j]	10% SO_3/H_2SO_4	220	500	SO_3	CH_3OSO_3H	43	81	~36	>500	(*6, 43*)
Ir(COD)Cl/dmpe [k]	Cyclohexane	150	500	B_2pin_2 [l]	CH_3Bpin [m]	~52	–	~6.5	104	(*44*)
Cp^*_2ScMe [o]	Cyclohexane	80	– [p]	$CH_3CH=CH_2$	$(CH_3)_3CH$	–	–	0.04	–	(*45*)
bis(NHC)$PdBr_2$ [q]	HTFA [c]	90	435	$K_2S_2O_8$	CH_3TFA [c]	–	–	2.4	–	(*46*)
$Ce(OTf)_4$ [r]	CH_3CN	25	725	CCl_3CH_2OH	Aryl and alkyl derivatives	29	NA	NA	2900	(*47*)
$RhCl_3$−NaCl−KI [s]	$H_2O_{(l)}/CF_3COOH_{(l)}$	95	870	H_2O_2/HOI [t]	C_1 [v]	–	–	[w]	–	(*48*)
Cu_3Etppz [x]	$H_2O_{(l)}$, $H_2O_{2(l)}$ [y]	25	14.5	O_2	CH_3OH	–	–	–	6.5	(*49*)

[a] TOF, turnover frequency. [b] TON, turnover number. [c] TFA, trifluoroacetate. [d] Obtained after hydrolysis from the immediate product, CH_3OSO_3H. [e] Total amount of CH_4 reacted. [f] Electrochemically generated high-valency Pd dimer during cyclic voltammetry. [g] Proposed yet not confirmed in this specific experiment. [j] Electrochemically generated high-valency Pd dimer during bulk electrolysis in the presence of CH_4. [j] bpym, bipyrimidine. [k] COD, 1,5-cyclooctadiene; dmpe, 1,2-bis(dimethylphosphino)ethane. [l] B_2pin_2, 4,4,4′,4′,5,5,5′,5′-Octamethyl-2,2′-bi-1,3,2-dioxaborolane. [m] CH_3Bpin, 2,4,4,5,5-pentamethyl-1,3,2-dioxaborolane. [o] Cp^*, cyclopentadiene. [p] Not reported. [q] NHC, N-Heterocyclic carbenes. [r] Photocatalytic system; OTf, trifluoromethanesulfonate. [s] Represents starting materials in solution. [t] O_2 and CO are bubbled in and facilitate generation of peroxide species. [u] Proposed oxidants generated in solution. [v] CH_3OH and CF_3COOH, CH_3COOH, HCOOH, and CO_2 were all observed. [w] 71, 9, 12, and 1300 corresponding to CH_3OH and CF_3COOH (combined), CH_3COOH, HCOOH, and CO_2, respectively. [x] Cu_3Etppz, 3,30 -(1,4-diazepane1,4-diyl)bis[1-(4-ethylpiperazine-1-yl)propan-2-ol]). [y] H_2O_2 is added at 20 equivalents to regenerate the catalyst.

Table S3. Reactivities of reported heterogeneous catalysts for methane functionalization

Catalyst	Solvent/phase	T (°C)	P_{CH4} (psi)	Oxidant	Product	Yield (%)	Selectivity (%)	TOF [a] (hr^{-1})	TON [b]	Ref.
AuPd NP [c]	$H_2O_{(l)}$	50	435	O_2/H_2O_2	CH_3OH	–	92	–	–	(*50*)
Cu-zeolite	$He_{(g)}$ or $O_{2(g)}$, $CH_{4(g)}$, $H_2O_{(g)}$ [d]	400, 200 [d]	102	H_2O	CH_3OH	–	~97	–	0.204 [e]	(*51*)
Ga_2O_3/MoO_3	$CH_{4(g)}/He_{(g)}/ O_{2(g)}$	455	334	O_2	CH_3OH	66	22	–	–	(*52*)
ZSM-5	$H_2O_{(l)}$	50	442	H_2O_2	CH_3OH	–	12	6320	>3000	(*53*)
Cu-ZSM-5	$H_2O_{(l)}$	50	442	H_2O_2	CH_3OH	–	83	2113	>1057	(*53*)
Fe-silicalite-1	$H_2O_{(l)}$	70	43.5	H_2O_2	CH_3OH	–	93	70	>35	(*53*)
Fe-ZSM-5	$CH_{4(g)}/ N_2O_{(g)}$	160	<1	N_2O	CH_3OH	70	76	–	3.6 [f]	(*54*)
FeO_x/TiO_x [g]	$CH_{4(g)}$	25	14.5	H_2O_2	CH_3OH	97	90	–	18	(*55*)
Cu-MOF-808	$N_2O_{(g)}$ /$He_{(g)}$, $CH_{4(g)}$ $He_{(g)}/H_2O_{(g)}$ [h]	150	14.5	N_2O	CH_3OH	–	–	–	71.8 [i]	(*56*)
FeN_4 in graphene [j]	$H_2O_{(l)}/ CH_{4(g)}$	25	290	H_2O_2	C_1 [k]	–	–	0.47	–	(*57*)
Cu-Fe-ZSM-5	$CH_{4(g)}/ N_2O_{(g)}$	342	14.5	N_2O	CH_3OH	–	78	–	–	(*58, 59*)
Rh-ZSM-5 [l]	$CH_{4(g)}/CO_{(g)}/ O_{2(g)}$	150	290	O_2	$C_{1,2}$ [m]	–	–	–	[n]	(*60*)
CuEtp@AlMSN30-ex [o]	$CH_{4(g)}/H_2O_{(l)}$, $H_2O_{2(l)}$ [p]	25	14.5	O_2	CH_3OH	–	–	–	171.2	(*61*)
CZ-12–0.58 [q]	$O_{2(g)}$, $He_{(g)}$, $CH_{4(g)}$ [r]	170	14.5	O_2	CH_3OH	–	98	–	8.2 [s]	(*62*)
Cu-MOR	$O_{2(g)}$, $CH_{4(g)}$, $H_2O_{(l)}$ [t]	200	14.5	O_2	$C_{1,2}$ [u]	–	–	–	160 [v]	(*63*)
FeZSM-5	$O_{2(g)}$, $N_2O_{(g)}$, $CH_{4(g)}$, [w]	25	14.5	N_2O	$C_{1,2}$ [u]	70 [x]	–	–	–	(*64*)
Co-ZSM-5-*at*-1-20 [y]	$O_{2(g)}/ CH_{4(g)}$ [z]	150	14.5	O_2	C_1 [aa]	–	75	–	2.25 [bb]	(*65*)
Cu-H-ZSM-5 [cc]	$O_{2(g)}/CH_{4(g)}/ H_2O_{(g)}$	210	14.2	O_2	C_1 [dd]	–	–	–	82 [ee]	(*66*)
Cu-Na-ZSM-5 [cc, ff]	$O_{2(g)}/CH_{4(g)}/ H_2O_{(g)}$	210	14.2	O_2	C_1 [dd]	–	71	–	37 [gg]	(*66*)
Ni-ZSM5 [hh]	$O_{2(g)}/CH_{4(g)}/ H_2O_{(g)}$	175	14.5	O_2	$C_{1,2}$ [ii]	–	–	–	5.1 [jj]	(*67*)

[a] TOF, turnover frequency. [b] TON, turnover number. [c] AuPd nanoparticles supported on polyvynil pyridine. [d] Cyclic operation. [e] Moles of CH_3OH per mole of Cu in zeolite. [f] Quasicatalytic due to insufficient temperatures for desorption [g] Photocatalysis under 1-sun illumination. [h] The catalyst was pretreated with 3 % N_2O in He for 2 hrs (150 °C), purged with He for 30 min, exposed to CH_4 for 1 hr (150 °C), and introduced to 3 % steam in He (150 °C) to desorb CH_3OH. [i] Moles of CH_3OH per mole of Cu in MOF. [j] Single Fe atom sites confined in graphene [k] CH_3OH, CH_3OOH, $HOCH_2OOH$, and HCOOH were all observed. [l] Rh-ZSM-5 is pretreated with 5 % H_2 at

550 °C for 3 hrs. [m] CH_3OH, CH_3COOH, HCOOH, and CO_2 were all observed. [n] 2068, 21295, 7020, and 5010 corresponding to µmol product per gram catalyst for CH_3OH, CH_3COOH, HCOOH, and CO_2, respectively. [o] CuEtp, $Cu^ICu^ICu^I$(3,3-(1,4-diazepane1,4-diyl)bis[1-(4-ethylpiperazine-1-yl)propan-2-ol]), stabilized on pore-expanded mesoporous silica nanoparticles with Al-doping (Si/Al ratio = 30). [p] H_2O_2 is added at 200 equivalents to regenerate the catalyst. [q] CZ-12–0.58, Cu-ZSM-5 with Si/Al ratio = 12 and Cu/Al ratio = 0.58. [r] CZ-12–0.58 is pretreated with O_2 at 450 °C, cooled to room temperature, flushed with He, and CH_4 was passed over as the temperature was increased to 170 °C. [s] Corresponds to µmol CH_3OH per gram CZ-12–0.58. [t] Catalyst is pretreated with O_2 at 450 °C, reacted with CH_4, and purged with H_2O to desorb product. [u] Dimethyl ether and CH_3OH were both observed. [v] Corresponds to µmol product, dimethyl ether and CH_3OH, per gram Cu-MOR. [w] FeZSM-5 was pretreated with O_2 at 550 °C, then heated to 900 °C under vacuum, and finally treated with N_2O at 230 °C prior to use. [x] CH_3OH was extracted with ethanol for multiple cycles [x] Sample was treated with NaOH, where 1 signifies the [NaOH] and 20 the reaction time in mins. [z] Catalyst was exposed to O_2 and CH_4 and then treated with ethanol to recover the products. [aa] CH_3OH and HCOOH were both observed. [bb] Corresponds to µmol of CH_3OH per gram Co-ZSM-5-*at*-1-20 and was estimated from a bar graph. [cc] Catalyst is pretreated for 5 hrs at 550 °C with flowing O_2, cooled to 210 °C under O_2 flow and then purged under He for 0.5 hrs. Cu/Al = 0.31. [dd] Both CH_3OH and CO_2 were observed. [ee] µmol of CH_3OH per gram Cu-H-ZSM-5. [ff] Cu/Al = 0.37, Na/Al = 0.26. [gg] µmol of CH_3OH per gram Cu-Na-ZSM-5 [hh] 5 wt % Ni on ZSM5. The catalyst is activated at 650 °C with pure O_2 for 3 hrs. Ni/Al = 1. [ii] CH_3OH, HCOOH, and $HOCH_2CH_2OH$ were all observed as products. [jj] µmol of CH_3OH per gram Ni-ZSM5.

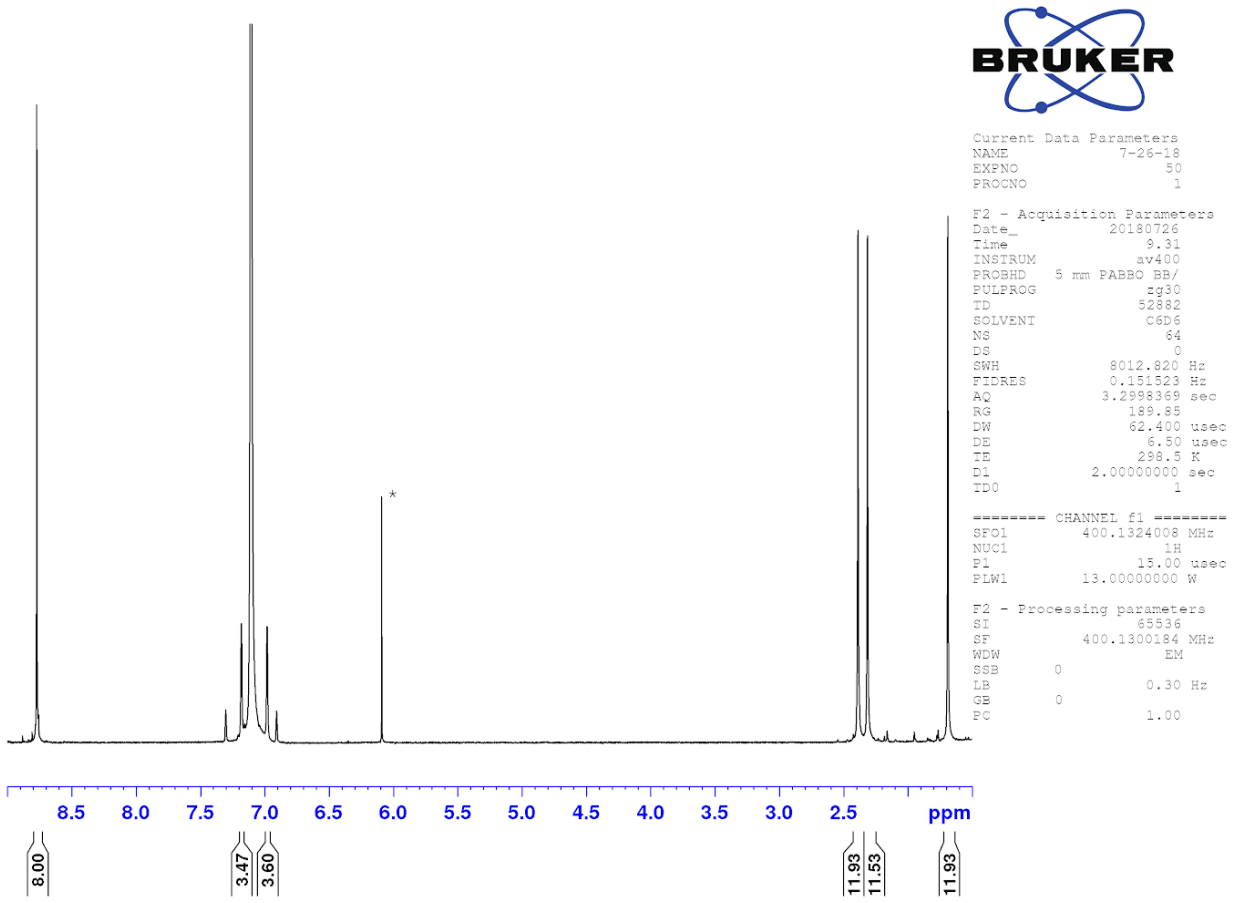

Figure S1. ^{1}H NMR spectrum of **1d** in C_6D_6. All integrations are referenced to the peak at 8.77 ppm. The solvent peak, C_6D_6, appears at 7.09 ppm. The marked * peak is due to residual $CHCl_3$.

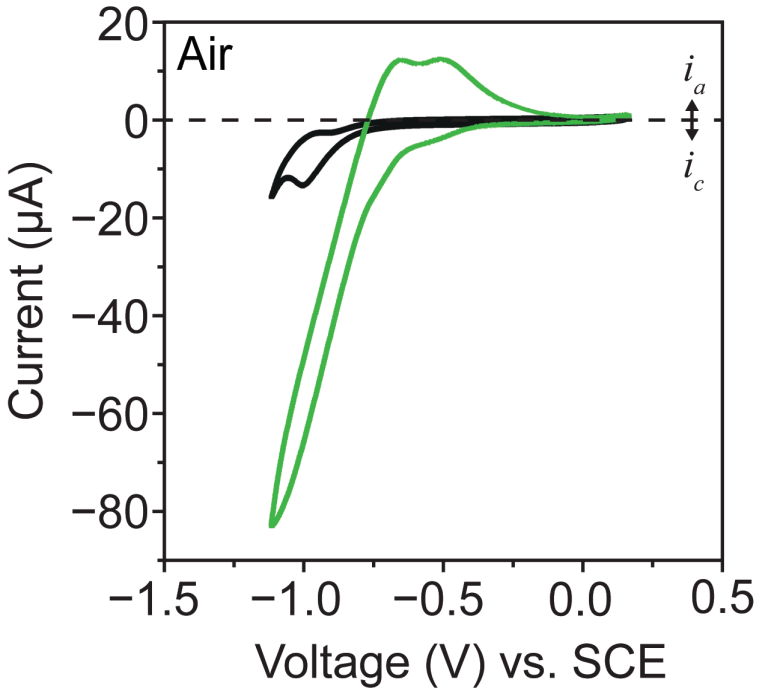

Figure S2. Cyclic voltammograms on glassy carbon electrodes in ambient air. Black trace, blank without the addition of **1d**; green trace, 1 mM **1d**. 0.1 M $TBAClO_4$ in 1,2-DFB, 100 mV/s.

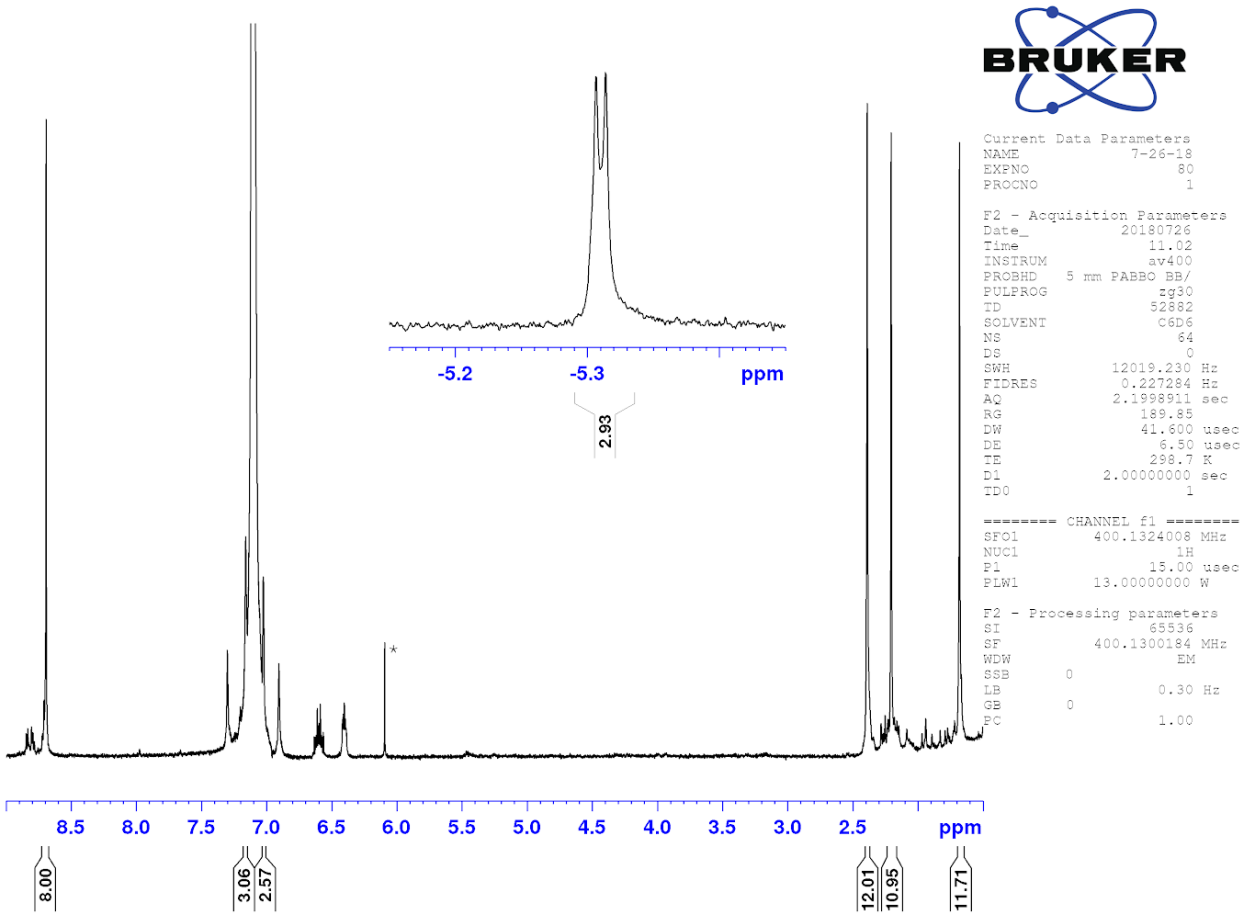

Figure S3. ^{1}H NMR spectrum of **1b** in C_6D_6. All integrations are referenced to the peak at 8.69 ppm. The solvent peak, C_6D_6, appears at 7.10 ppm. The marked * peak is due to residual $CHCl_3$.

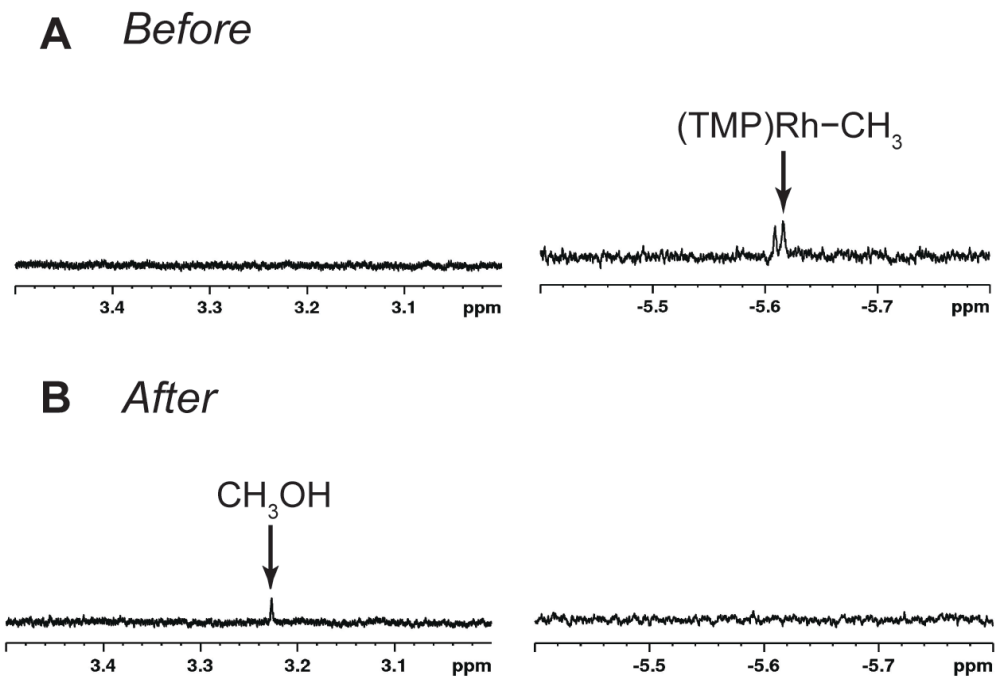

Figure S4. ^{1}H NMR spectra of **1b** with *t*-butyl hydroperoxide (**A**) upon mixing and (**B**) after 6 hrs at ambient conditions. Solvent: 80% 1,2-DFB and 20% C_6D_6. TMS was added as the internal reference after the reaction.

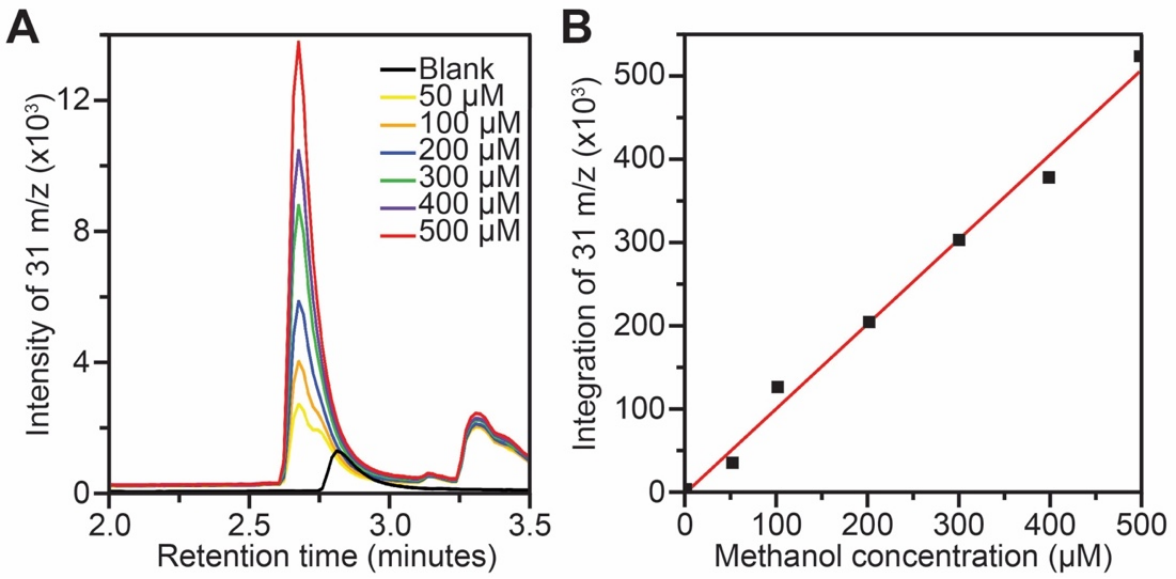

Figure S5. (**A**) a gas chromatograph spectrum monitoring a m/z ratio of 31 with varying concentrations of CH_3OH. The observed retention time is at about 2.62 min. (**B**) calibration curve of CH_3OH concentration and its corresponding integration of the 31 m/z on the chromatograph at the abovementioned retention time.

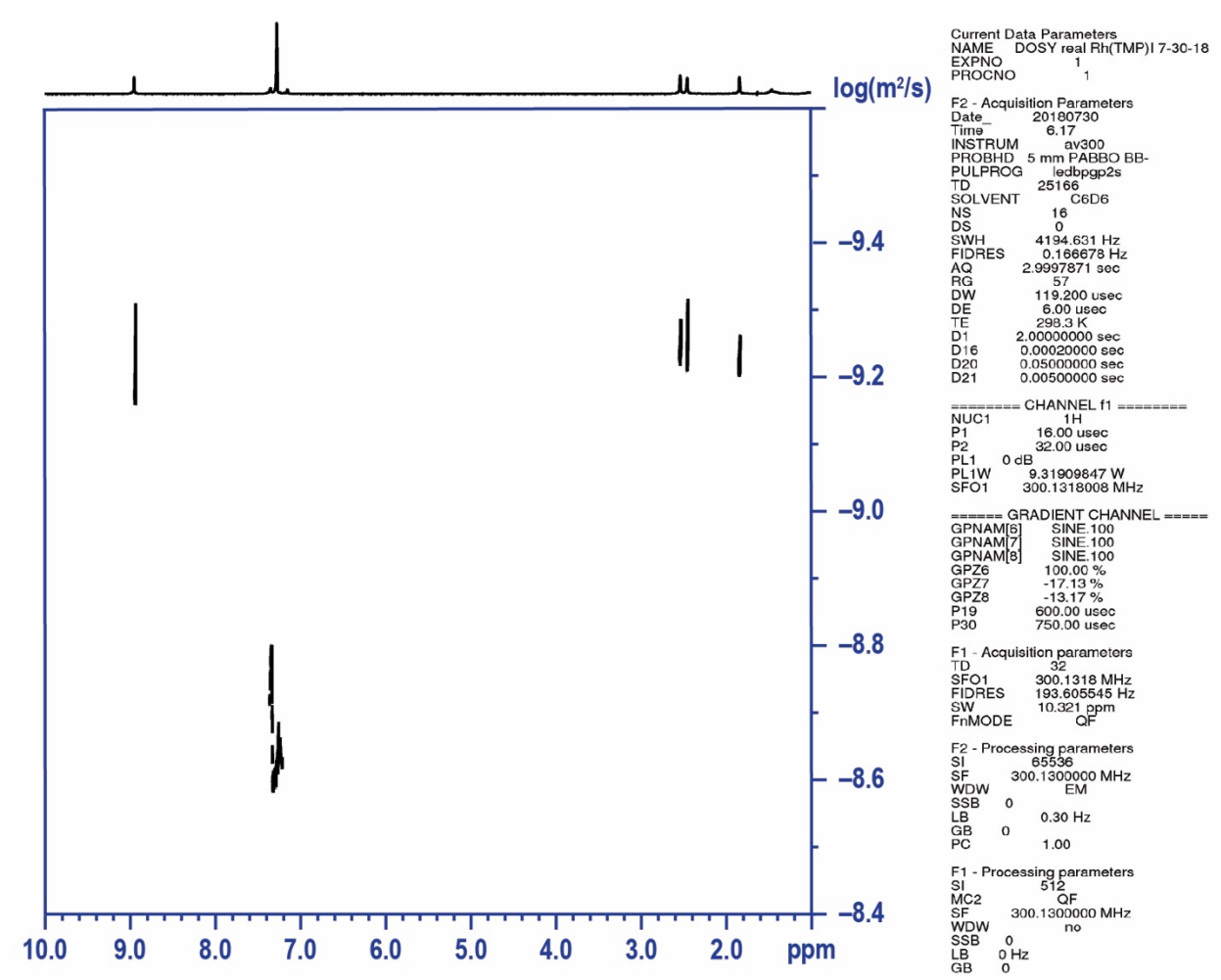

Figure S6. DOSY ^{1}H NMR spectrum of **1d** in C_6D_6. The major peaks of **1d** appear at 1.88, 2.47, 2.58, and 8.96 ppm. The largest peak is due to solvent and appears at 7.37 ppm. The diffusion coefficient of **1d** is determined to be 5.62×10^{-10} $m^2 \cdot s^{-1}$.

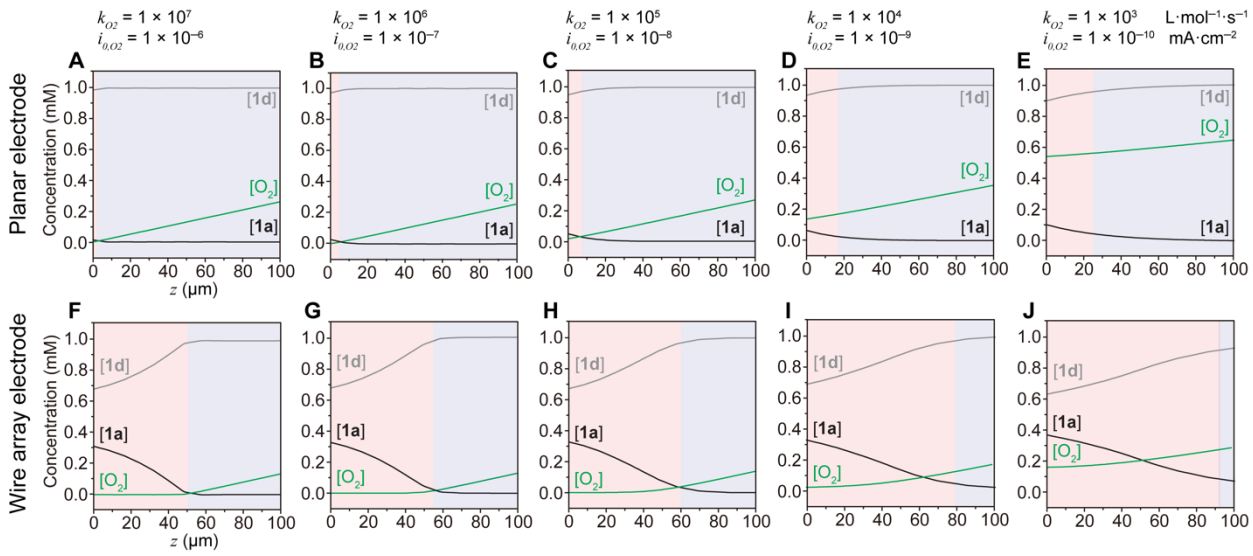

Figure S7. Simulation results of concentrations of **1a**, **1d** and O_2, denoted as [**1a**], [**1d**] and [O_2] on a wire array electrode (50 μm length, 4 μm diameter and 15 μm periodicity) respectively, versus the distance away from the bottom of array (*z*). (**A**) to (**E**), planar electrode; (**F**) to (**J**), wire array electrode. The region with the accumulation of CH_4-reactive **1a** is colored in pink, while the aerobic region in blue. The electrode geometry is the same among **f** to **j**. k_{O2}, the second-order reaction rate constant between O_2 and **1a**; $i_{0,O2}$, the exchange current density for the reduction of O_2. (**A**) and (**F**), $k_{O2} = 1\times10^{7}$ L·mol^{-1}·s^{-1}, $i_{0,O2} = 1\times10^{-6}$ mA/cm^2; (**B**) and (**G**), same as Figures 3A and 3B, $k_{O2} = 1\times10^{6}$ L·mol^{-1}·s^{-1}, $i_{0,O2} = 1\times10^{-7}$ mA/cm^2; (**C**) and (**H**), $k_{O2} = 1\times10^{5}$ L·mol^{-1}·s^{-1} $i_{0,O2} = 1\times10^{-8}$ mA/cm^2; (**D**) and (**I**), $k_{O2} = 1\times10^{4}$ L·mol^{-1}·s^{-1}, $i_{0,O2} = 1\times10^{-9}$ mA/cm^2; (**E**) and (**J**), $k_{O2} = 1\times10^{3}$ L·mol^{-1}·s^{-1}, $i_{0,O2} = 1\times10^{-10}$ mA/cm^2.

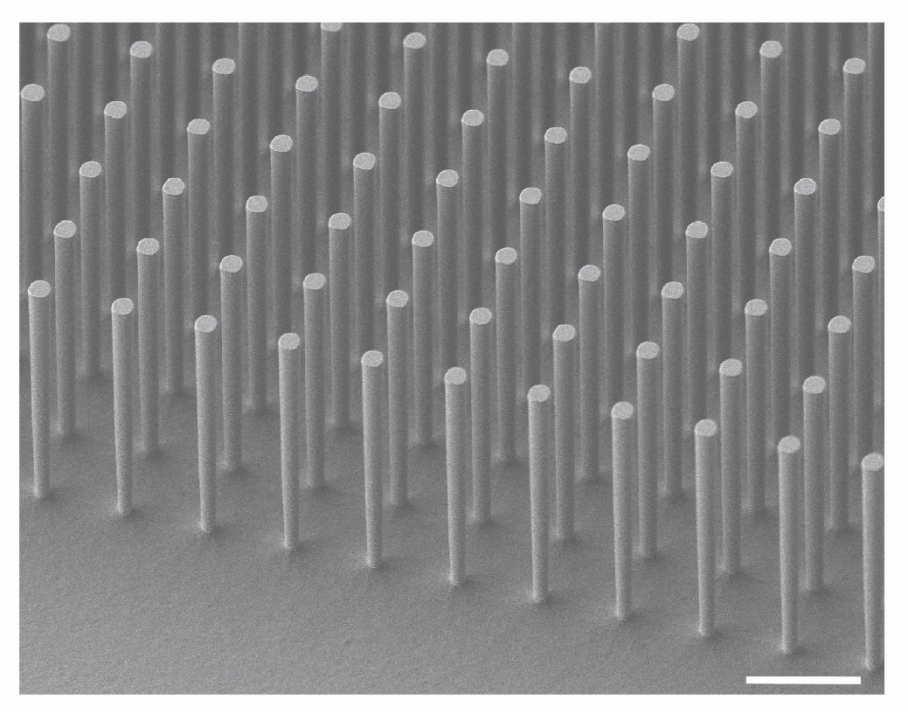

Figure S8. 45°-tilting SEM image of Si wire array used for optical mapping of concentration gradient. The scale bar, 20 μm.

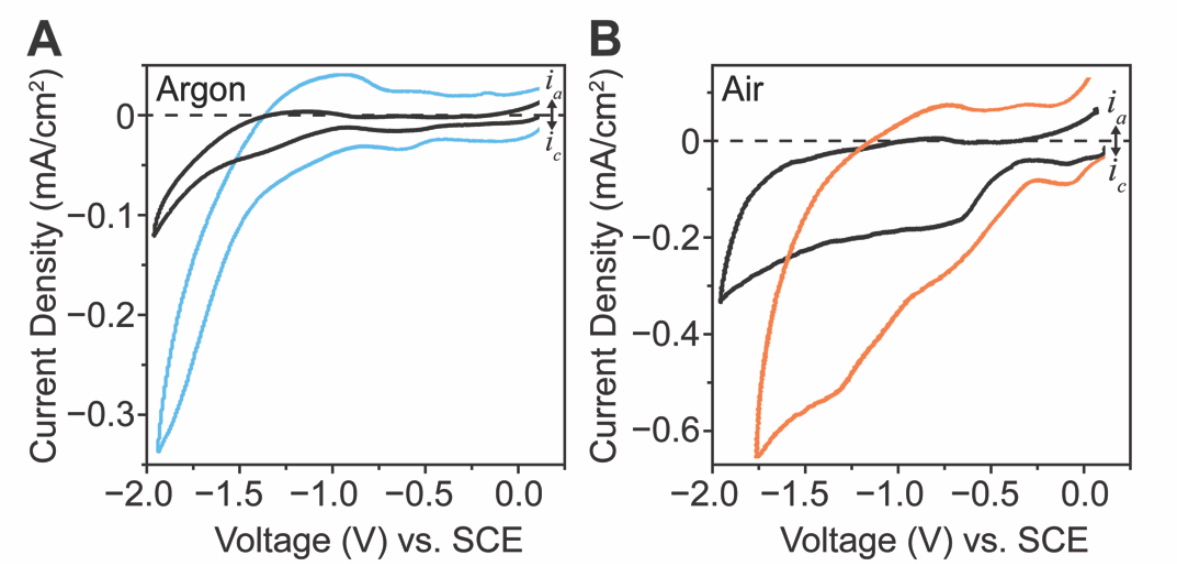

Figure S9. Cyclic voltammograms on Si wire electrodes in Ar (**A**) and air (**B**). Black trace, blank without the addition of **1d**; blue and orange traces, 1 mM **1d**. 0.1 M $TBAClO_4$ in 1,2-DFB, 100 mV/s.

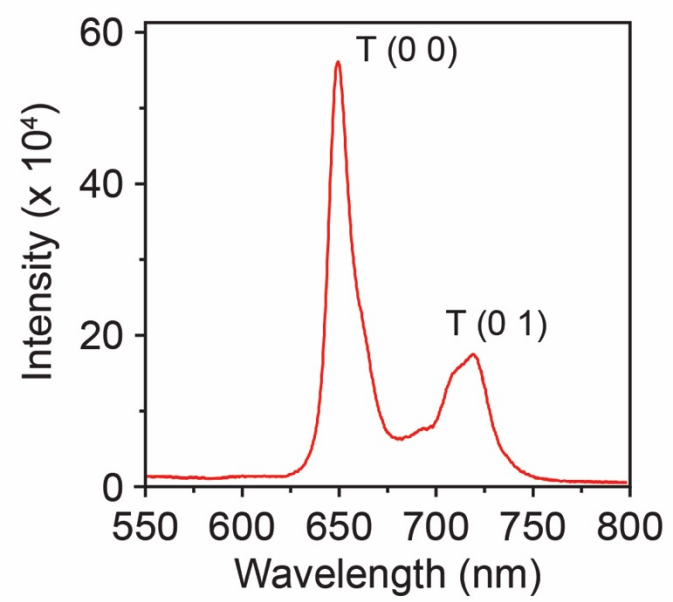

Figure S10. Phosphorescence emission spectrum of **1d** under a 526-nm excitation. The assignment of transitions from the triplet states are listed.[68]

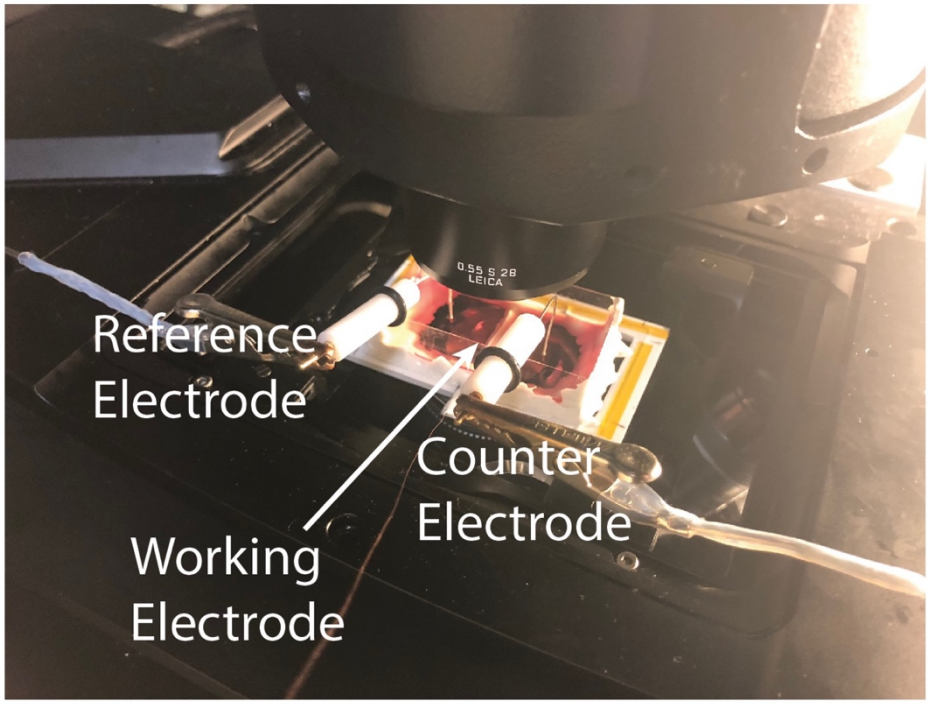

Figure S11. Photograph of an electrochemical setup used for *in situ* mapping of phosphorescence emission under a confocal optical microscope.

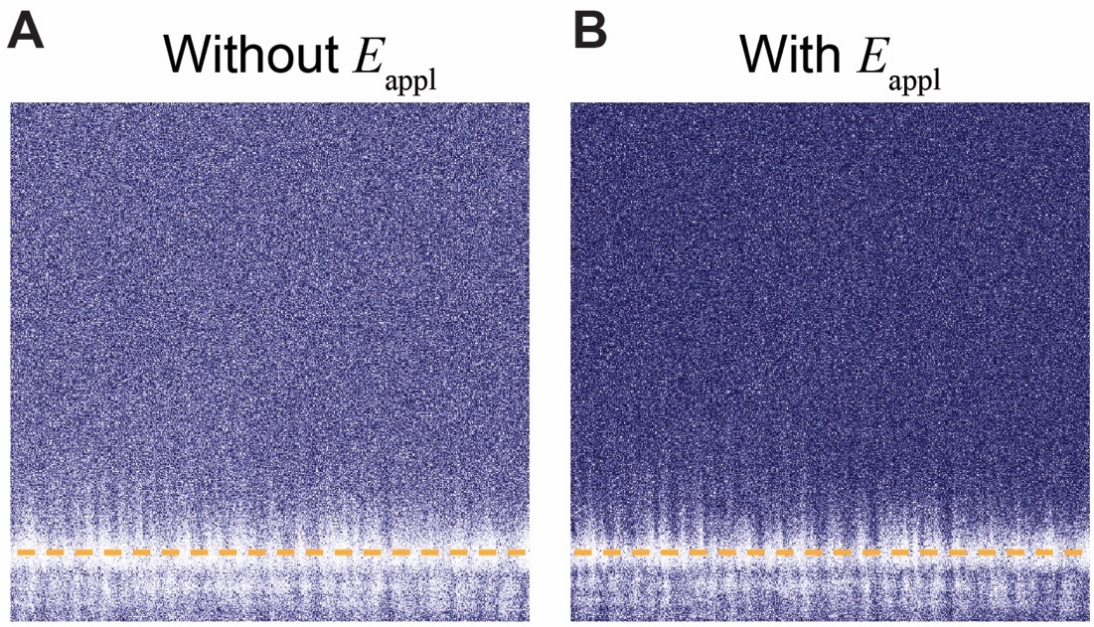

Figure S12. Cross-sectional heatmaps of unnormalized phosphorescence intensity on a planar electrode without (**A**) and with (**B**) E_{appl}. The surface of Si planar electrode is delineated in yellow. No significant concentration gradient was built near a planar electrode despite a uniform background change. 0.1 mM **1d** in the bulk solution, 0.1 M $TBAClO_4$ in 1,2-DFB, E_{appl} = −1.5 V vs. SCE.

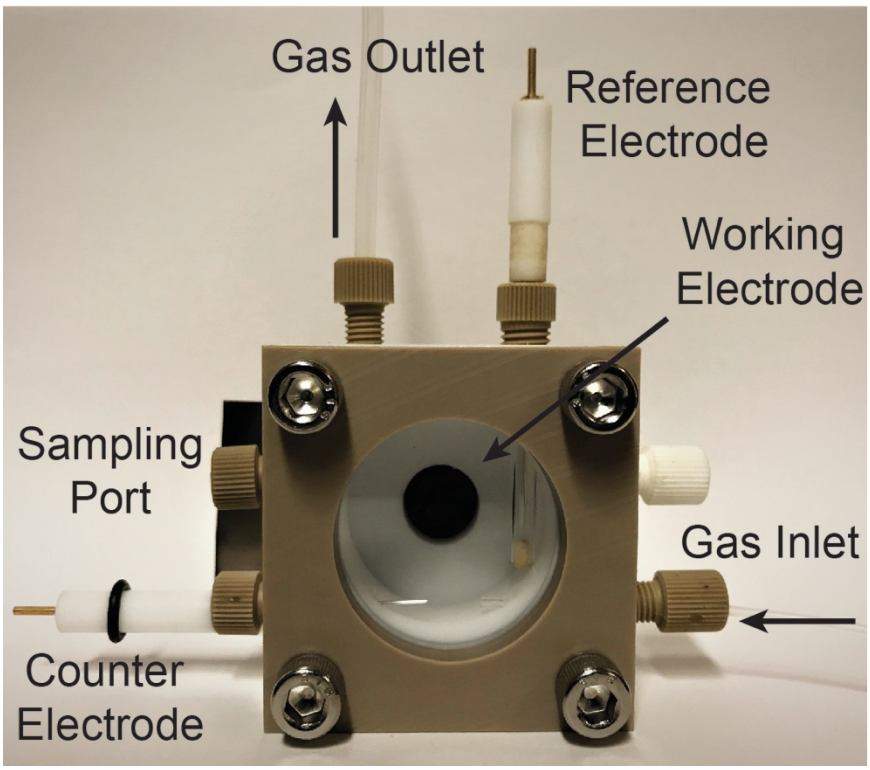

Figure S13. Photograph of the customized electrochemical reactor used for bulk electrolysis.

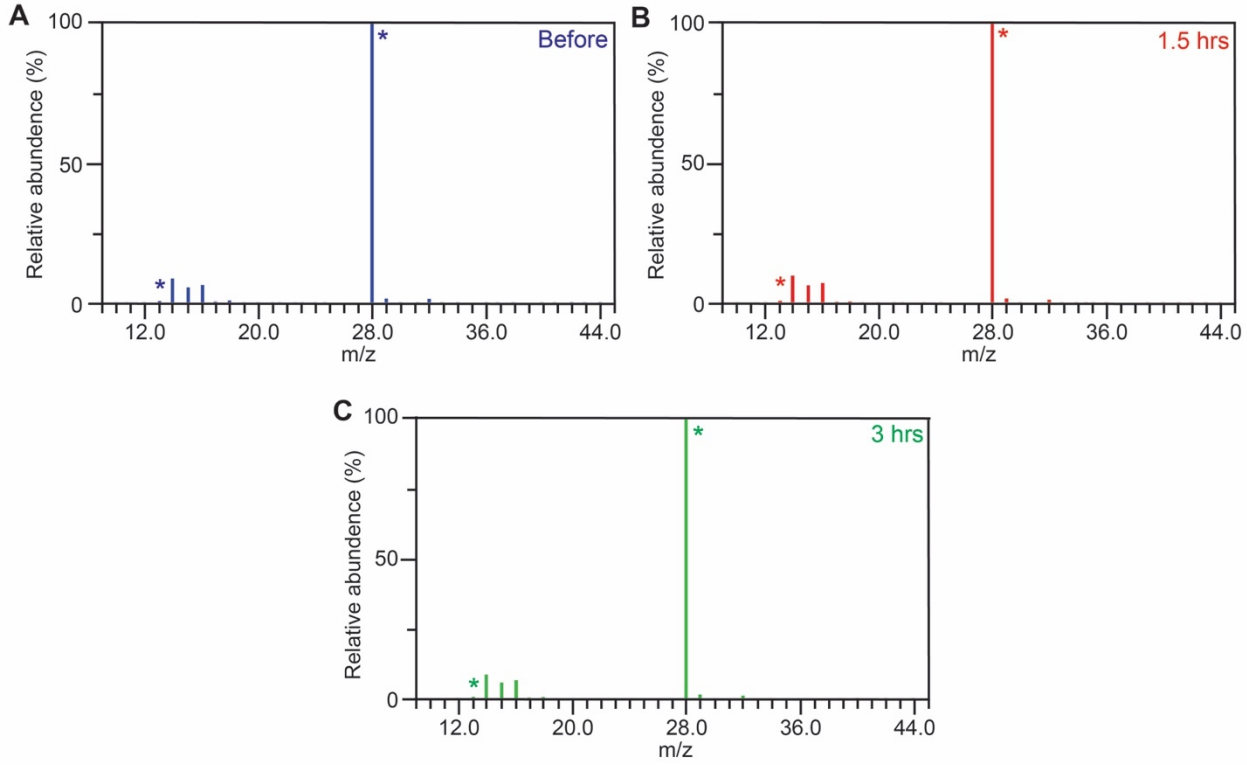

Figure S14. Mass spectra of gas samples taken before the bulk electrolysis (**A**), as well as 1.5 hrs (**B**) and 3 hrs (**C**) after the commencement of bulk electrolysis. The marked peaks, at m/z ratios of 14 and 28, correspond to the fragments of N_2. CO was monitored at an m/z fragment of 12 and CO_2 was monitored at a fragment of 44 m/z. CO and CO_2 were not detectable as products during the bulk electrolysis.

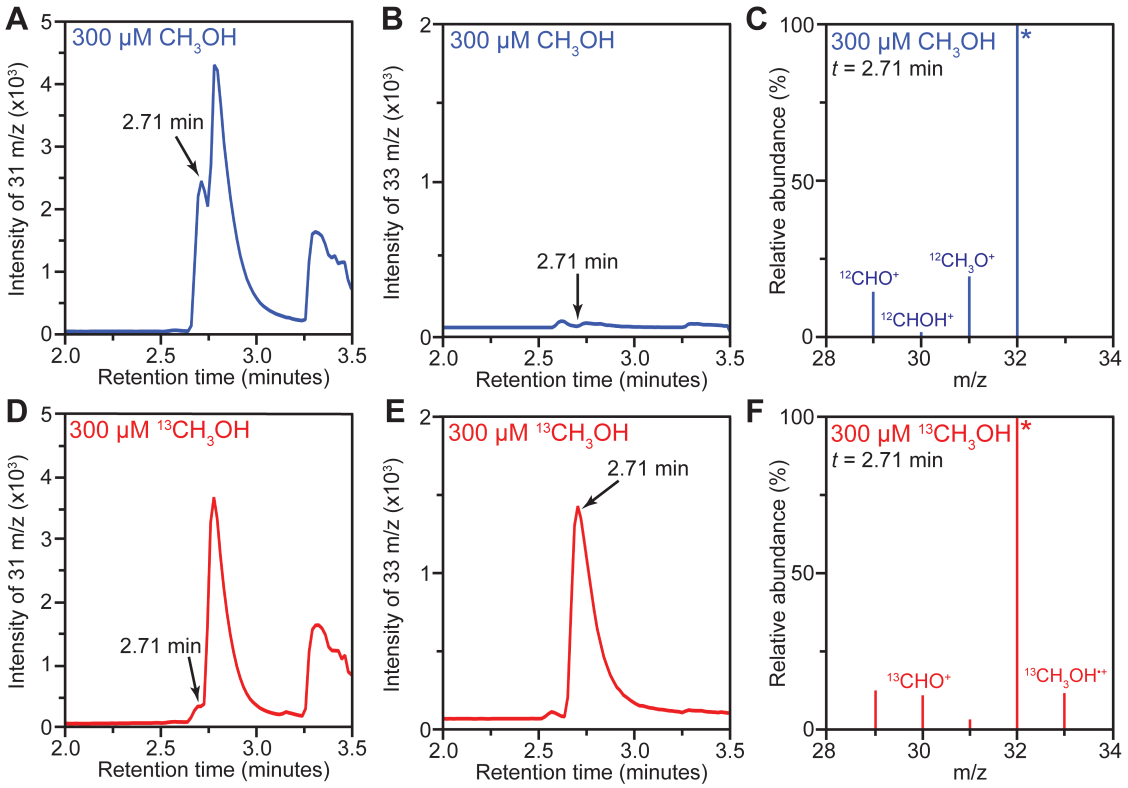

Figure S15. GC-MS elusion traces when monitored at m/z = 31 (**A** and **D**) or at m/z = 33 (**B** and **E**) for CH_3OH of natural abundance and $^{13}CH_3OH$, respectively. The mass spectra at an elution time of 2.71 min, the position of CH_3OH peaks, were also displayed for CH_3OH of natural abundance (**C**) and $^{13}CH_3OH$ (**F**).

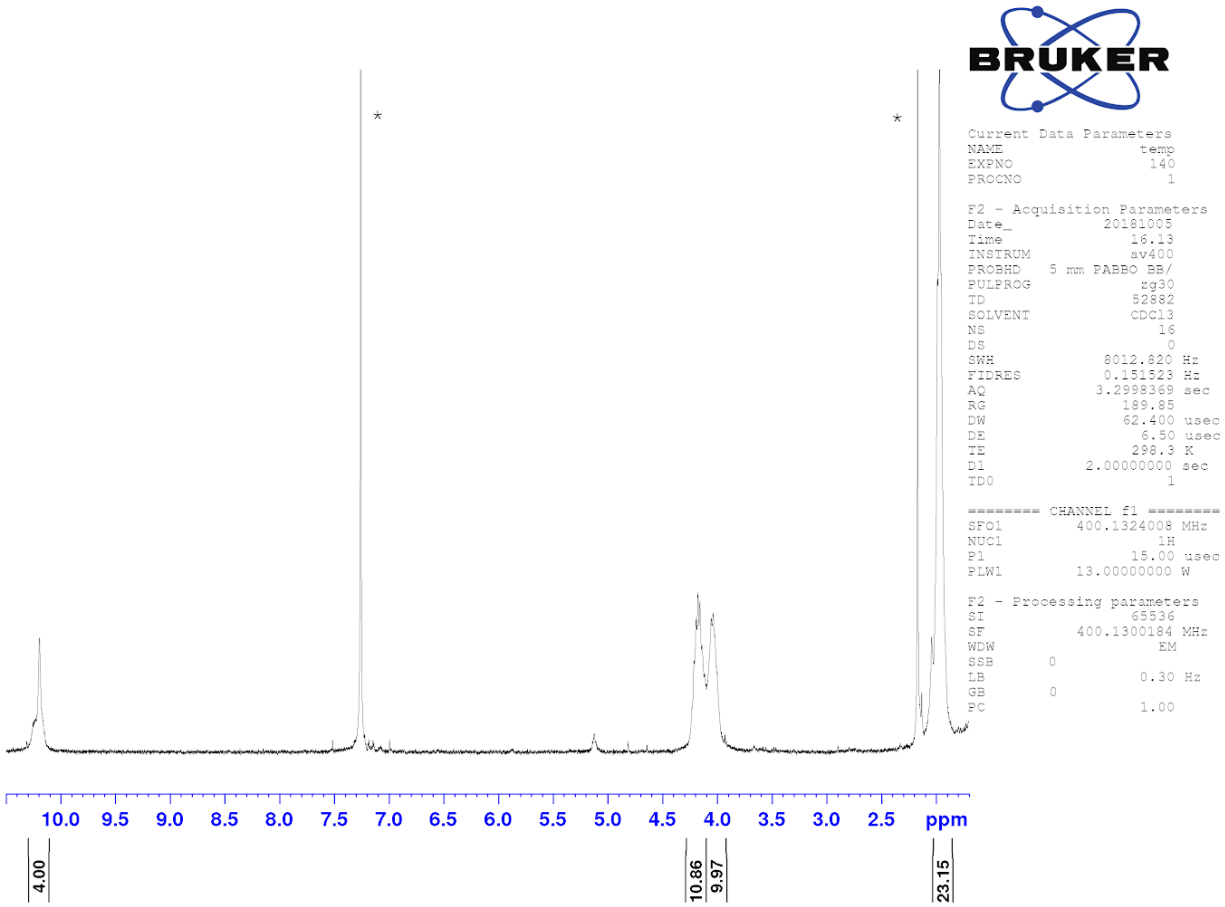

Figure S16. ^{1}H NMR spectrum of **2** in $CDCl_3$. All integrations are referenced to the peak at 10.28 ppm. The solvent peak, $CDCl_3$, appears at 7.27 ppm. The marked peaks are due to solvent, $CHCl_3$, and residual acetone.

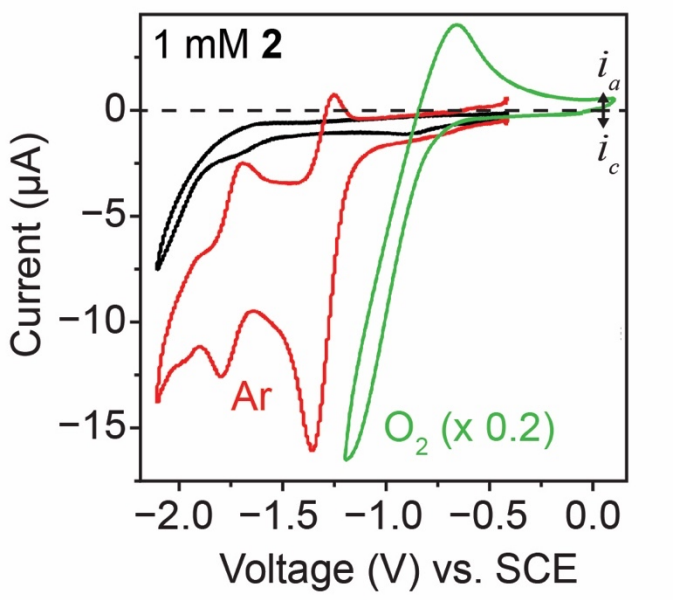

Figure S17. Cyclic voltammograms of 1 mM **2** with 0.1 M $TBAClO_4$ in 1,2-DFB under Ar (red) and air (green) environment. Black, blank solution without **2**. 100 mV/s; Pt working electrode for blank and in Ar, glassy carbon electrode in air. The current in O_2 is multiplied by a factor of 0.2.

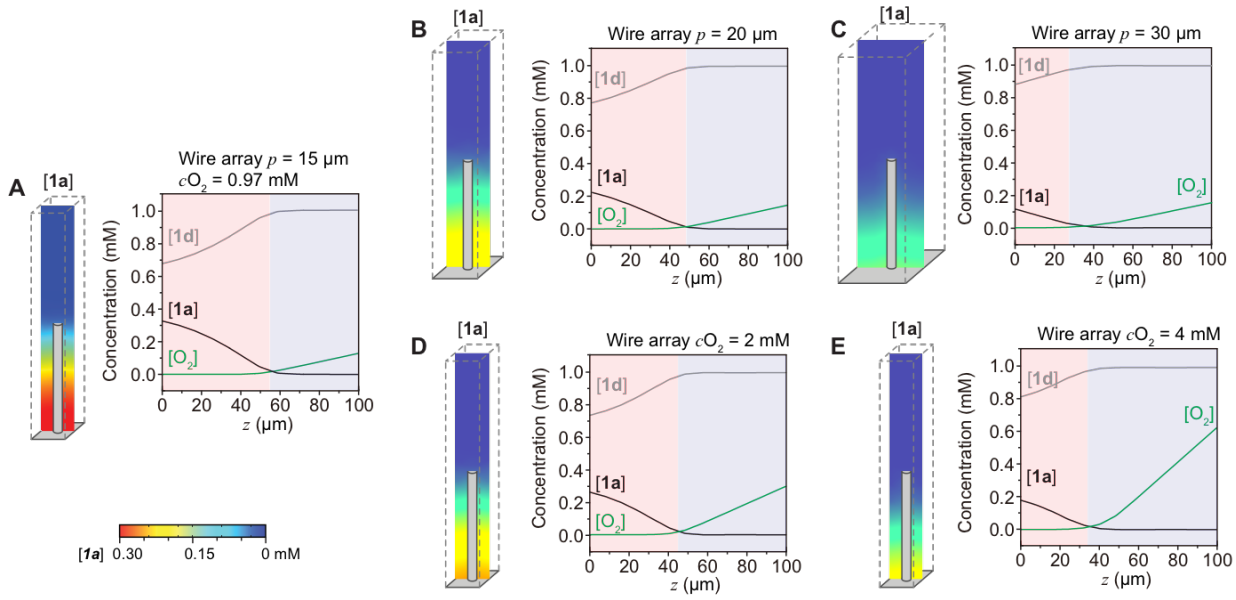

Figure S18. (**A**) to (**E**), simulation results of wire arrays with different periodicities of wire array (p) and bulk O_2 concentrations (C_{O2}). The concentrations of **1a**, **1d** and O_2, denoted as [**1a**], [**1d**] and [O_2] respectively, were plotted versus the distance away from electrode surface (z). The region with the accumulation of CH_4-reactive **1a** is colored in pink, while the aerobic region in blue. (**A**), same as Figure 2B, whose conditions corresponds to a 0.1 bar partial pressure of O_2.

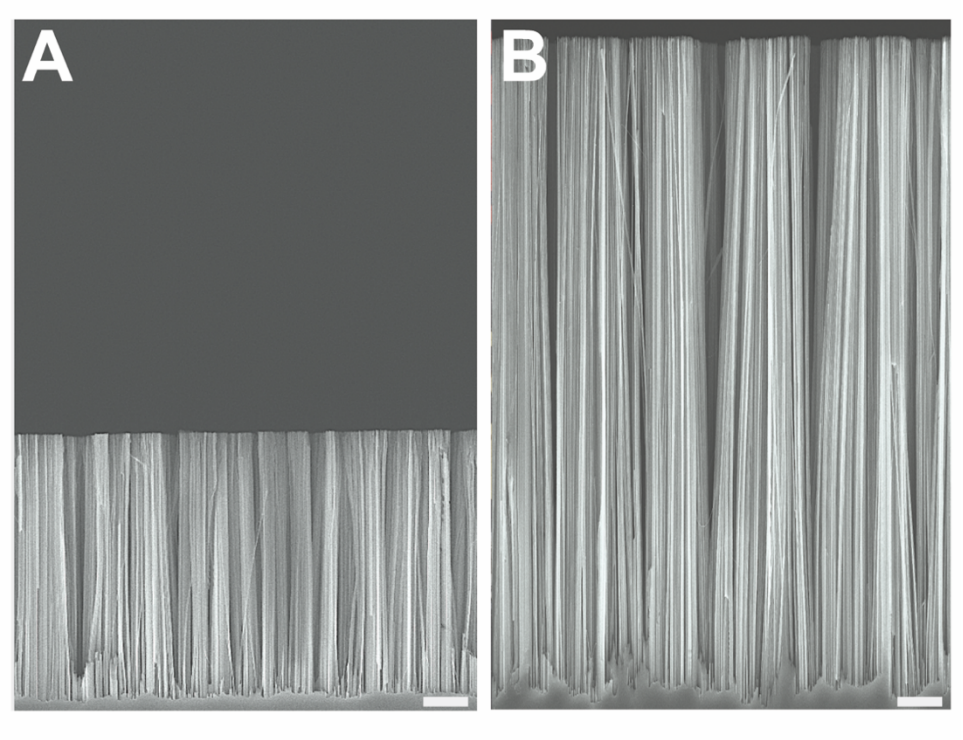

Figure S19. SEM images of (**A**) 10-μm and (**B**) 27-μm Si nanowire arrays. The scale bars in both images correspond to 2 μm.

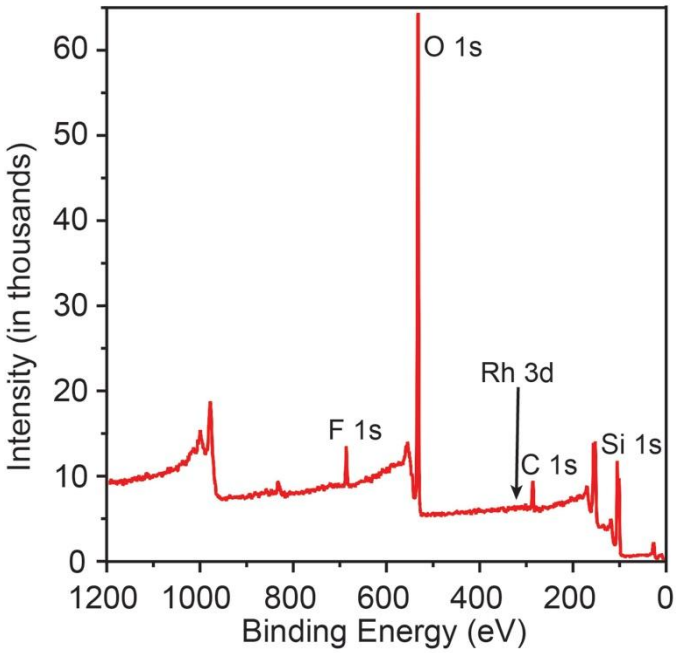

Figure S20. Spectrum of X-ray photoelectron spectroscopy for the surface of Si nanowire after a 3-hr bulk electrolysis with the condition of entry *23* in Table S1.

Additional references

(36) Bard, A. J.; Faulner, L. R. Electrochemical Methods: Fundamentals and Applications. 2nd ed. John Wiley & Sons, Inc., New York, **2001**.

(37) Xiang,C.; Meng, A. C.; Lewis, N. S. Evaluation and optimization of mass transport of redox species in silicon microwire-array photoelectrodes. *Proc. Natl. Acad. Sci. U. S. A.* **2012**, *109*, 15622−15627.

(38) Sato, T.; Hamada, Y.; Sumikawa, M.; Araki, S.; Yamamoto, H. Solubility of Oxygen in Organic Solvents and Calculation of the Hansen Solubility Parameters of Oxygen. *Ind. Eng. Chem. Res.* **2014**, *53*, 19331−19337.

(39) Schumpe, A.; Luehring, P. Oxygen diffusivities in organic liquids at 293.2 K. *J. Chem. Eng. Data* **1990**, *35*, 24−25.

(40) Zimmermann, T.; Soorholtz, M.; Bilke, M.; Schüth, F. Selective Methane Oxidation Catalyzed by Platinum Salts in Oleum at Turnover Frequencies of Large-Scale Industrial Processes. *J. Am. Chem. Soc.* **2016**, *138*, 12395−12400.

(41) Hashiguchi, B. G., *et al.* Main-Group Compounds Selectively Oxidize Mixtures of Methane, Ethane, and Propane to Alcohol Esters. *Science* **2014**, *343*, 1232−1237.

(42) Periana, R. A.; Mironov, O.; Taube, D.; Bhalla, G.; Jones, C. Catalytic, Oxidative Condensation of CH_4 to CH_3COOH in One Step via CH Activation. *Science* **2003**, *301*, 814−818.

(43) Mironov, O. A., *et al.* Using Reduced Catalysts for Oxidation Reactions: Mechanistic Studies of the "Periana-Catalytica" System for CH_4 Oxidation. *J. Am. Chem. Soc.* **2013**, *135*, 14644−14658.

(44) Smith, K. T., *et al.* Catalytic borylation of methane. *Science* **2016**, *351*, 1424−1427.

(45) Sadow, A. D.; Tilley, T. D. Homogeneous Catalysis with Methane. A Strategy for the Hydromethylation of Olefins Based on the Nondegenerate Exchange of Alkyl Groups and σ-Bond Metathesis at Scandium. *J. Am. Chem. Soc.* **2003**, *125*, 7971−7977.

(46) Meyer, D., *et al.* Palladium Complexes with Pyrimidine-Functionalized N-Heterocyclic Carbene Ligands: Synthesis, Structure and Catalytic Activity. *Organometallics* **2009**, *28*, 2142−2149.

(47) Hu, A.; Guo, J.-J.; Pan, H.; Zuo, Z. Selective functionalization of methane, ethane, and higher alkanes by cerium photocatalysis. *Science*, **2018**, *361*, 668−672.

(48) Chepaikin, E. G.; Bezruchenko, A. P.; Leshcheva, A. A.; Boyko, G. N.; Kuzmenkov, I. V.; Grigoryan, E. H.; Shilov, A. E. Functionalisation of methane under dioxygen and carbon monoxide catalyzed by rhodium complexes: oxidation and oxidative carbonylation. *J. Mol. Cat. A: Chemical* **2001**, *169*, 89−98.

(49) Chan, S. I.; Lu, Y.-J.; Nagababu, P.; Maji, S.; Hung, M.-C.; Lee, M. M.; Hsu, I.-J.; Minh, P. D.; Lai, J. C.-H.; Ng, K. Y.; Ramalingam, S.; Yu, S. S.-F.; Chan, M. K. Efficient Oxidation of Methane to Methanol by Dioxygen Mediated by Tricopper Clusters. *Ang. Chem., Int. Ed.*, **2013**, *52*, 3731−3735.

(50) Agarwal, N., *et al.* Aqueous Au-Pd colloids catalyze selective CH_4 oxidation to CH_3OH with O_2 under mild conditions. *Science* **2017**, *358*, 223−227.

(51) Sushkevich, V. L.; Palagin, D.; Ranocchiari, M.; van Bokhoven, J. A. Selective anaerobic oxidation of methane enables direct synthesis of methanol. *Science* **2017**, *356*, 523−527.

(52) Hutchings, G. J.; Taylor, S. H. Designing oxidation catalysts. *Catal. Today* **1999**, *49*, 105−113.

(53) Hammond, C., *et al.* Direct Catalytic Conversion of Methane to Methanol in an Aqueous Medium by using Copper-Promoted Fe-ZSM-5. *Angew. Chem., Int. Ed.* **2012**, *51*, 5129−5133.
(54) Starokon, E. V., *et al.* Oxidation of methane to methanol on the surface of FeZSM-5 zeolite. *J. Catal.* **2013**, *300*, 47−54.
(55) Xie, J., *et al.* Highly selective oxidation of methane to methanol at ambient conditions by titanium dioxide-supported iron species. *Nat. Catal.* **2018**, *1*, 889−896.
(56) Baek, J., *et al.* Bioinspired Metal–Organic Framework Catalysts for Selective Methane Oxidation to Methanol. *J. Am. Chem. Soc.* **2018**, *140*, 18208−18216.
(57) Cui, X., *et al.* Room-Temperature Methane Conversion by Graphene-Confined Single Iron Atoms. *Chem* **2018**, *4*, 1902−1910.
(58) Anderson, J. R.; Tsai, P. Methanol from oxidation of methane by nitrous oxide over FeZSM5 catalysts. *J. Chem. Soc., Chem. Commun.*, **1987**, *0* ,1435−1436.
(59) Tang, P.; Zhu, Q.; Wu, Z.; Ma, D. Methane activation: the past and future. *Energy Environ. Sci* **2014**, *7*, 2580−2591.
(60) Shan, J.; Li, M.; Allard, L. F.; Lee, S.; Flytzani-Stephanopoulos, M. Mild oxidation of methane to methanol or acetic acid on supported isolated rhodium catalysts. *Nature* **2017**, *551*, 605−608.
(61) Liu, C.-C.; Mou, C. Y.; Yu, S. S. F.; Chan, S. I. Heterogeneous formulation of the tricopper complex for efficient catalytic conversion of methane into methanol at ambient temperature and pressure. *Energy Environ. Sci***. 2016**, *9*, 1361−1374.
(62) Groothaert, M. H.; Smeets, P. J.; Sels, B. F.; Jacobs, P. A.; Schoonheydt, R. A. Selective Oxidation of Methane by the Bis(μ-oxo)dicopper Core Stabilized on ZSM-5 and Mordenite Zeolites. *J. Am. Chem. Soc.* **2005**, *127*, 1394−1395.
(63) Grundner, S.; Markovits, M. A. C.; Li, G.; Tromp, M.; Pidko, E. A.; Hensen, E. J. M.; Jentys, A.; Sanchez-Sanchez, M.; Lercher, J. A. Single-site trinuclear copper oxygen clusters in mordenite for selective conversion of methane to methanol. *Nat. Comm.* **2015**, *6*, 7546.
(64) Starokon, E. V.; Parfenov, M. V.; Pirutko, L. V.; Abornev, S. I.; Panov, G. I. Room-Temperature Oxidation of Methane by α-Oxygen and Extraction of Products from the FeZSM-5 Surface. *J. Phys. Chem. C* **2011**, *115*, 2155−2161.
(65) Beznis, N. V.; van Laak, A. N. C.; Weckhuysen, B. M.; Bitter, J. H. Oxidation of methane to methanol and formaldehyde over Co–ZSM-5 molecular sieves: Tuning the reactivity and selectivity by alkaline and acid treatments of the zeolite ZSM-5 agglomerates. *Micro. Meso. Mater.* **2011**, *138*, 176−183.
(66) Narsimhan, K.; Iyoki, K.; Dinh, K.; Román-Leshkov, Y. Catalytic Oxidation of Methane into Methanol over Copper-Exchanged Zeolites with Oxygen at Low Temperature. *ACS Centr. Sci***. 2016**, *2*, 424−429.
(67) Shan, J.; Huang, W.; Nguyen, L.; Yu, Y.; Zhang, S.; Yuanyuan Li, Y.; Frenkel, A. I.; Tao, F. Conversion of Methane to Methanol with a Bent Mono(μ-oxo)dinickel Anchored on the Internal Surfaces of Micropores. *Langmuir* **2014**, *30*, 8558−8569.
(68) Hanson, L. K.; Gouterman, M.; Hanson, J. C. Porphyrins. XXIX. Crystal and molecular structure and luminescence of bis(dimethylamine)etio(I)porphinatorhodium(III) chloride dihydrate. *J. Am. Chem. Soc.* **1973**, *95*, 4822−4829.